

KeyFace: Expressive Audio-Driven Facial Animation for Long Sequences via KeyFrame Interpolation

Antoni Bigata¹ Michał Stypułkowski² Rodrigo Mira¹ Stella Bounareli
Konstantinos Vougioukas¹ Zoe Landgraf¹ Nikita Drobyshev¹
Maciej Zieba³ Stavros Petridis¹ Maja Pantic¹

¹Imperial College London

²University of Wrocław

³Technical University of Wrocław

ab4522@imperial.ac.uk

Abstract

Current audio-driven facial animation methods achieve impressive results for short videos but suffer from error accumulation and identity drift when extended to longer durations. Existing methods attempt to mitigate this through external spatial control, increasing long-term consistency but compromising the naturalness of motion. We propose **KeyFace**, a novel two-stage diffusion-based framework, to address these issues. In the first stage, keyframes are generated at a low frame rate, conditioned on audio input and an identity frame, to capture essential facial expressions and movements over extended periods of time. In the second stage, an interpolation model fills in the gaps between keyframes, ensuring smooth transitions and temporal coherence. To further enhance realism, we incorporate continuous emotion representations and handle a wide range of non-speech vocalizations (NSVs), such as laughter and sighs. We also introduce two new evaluation metrics for assessing lip synchronization and NSV generation. Experimental results show that KeyFace outperforms state-of-the-art methods in generating natural, coherent facial animations over extended durations, successfully encompassing NSVs and continuous emotions.

1. Introduction

The field of audio-driven facial animation has advanced significantly with the development of generative models like Generative Adversarial Networks (GANs) [18] and Diffusion Models (DMs) [13, 22]. These approaches have greatly enhanced the realism and expressiveness of facial animations, enabling promising applications in virtual assistants, education, virtual reality, and aiding communication impairments [28, 34, 61]. As a result, the demand for high-resolution, natural, long-term audio-driven facial animations has increased dramatically.

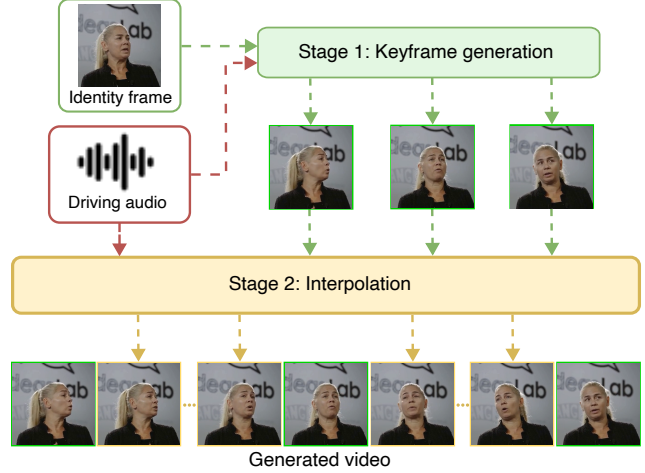


Figure 1. KeyFace generates long-term videos using a two-stage pipeline: first, keyframes are created as anchor points, then they are used by an interpolation model to produce smooth transitions.

While early approaches in audio-driven facial animation were limited in terms of head rotation [58] or focused solely on generating the mouth region [46], current methods have advanced to produce results that are nearly indistinguishable from real videos. Despite this progress, most methods struggle when handling longer audio inputs, suffering from identity drift and overall quality degradation beyond the initial few seconds [52, 65]. To extend generation length, some approaches incorporate additional spatial information, such as target head positions or landmarks, as model inputs [11, 56, 63]. While this can improve temporal consistency, it constrains animations to predefined facial motions, limiting expressiveness. Other methods use motion frames to provide context on prior movements [52, 65], but, as with many autoregressive approaches, small errors accumulate over time, reducing overall quality.

Furthermore, recent methods often neglect important as-

pects of long-form natural speech, such as continuously changing emotions and NSVs. Existing emotional audio-driven methods often assume a fixed emotional state [17, 27, 55], which restricts them to short sequences and overlooks real-world dynamics, where emotions fluctuate continuously. Moreover, they typically rely on discrete emotion labels [17, 19], which lack the nuance and fluidity of natural human expressions [62]. In contrast, the less-explored dimensions of valence and arousal provide a more precise portrayal of emotional states [2, 62]. Similarly, NSVs such as laughter and sighs are largely neglected, despite being essential for natural communication [45, 48]. Crucially, handling emotion and NSVs requires a model capable of interpreting them over extended sequences to accurately animate the corresponding facial expressions.

To address these limitations, inspired by keyframe-based approaches [67, 69] initially introduced by [43], we propose *KeyFace*, a novel two-stage approach for generating long and coherent audio-driven facial animations. In the first stage, a keyframe generation model produces a sequence at a low frame rate conditioned on an identity and audio input, spanning multiple seconds and eliminating the need for motion frames. In the second stage, an interpolation model fills in intermediate frames, ensuring smooth transitions and temporal coherence. By dividing generation into two parts, we implicitly separate motion and identity control, resulting in more natural motion and improved identity preservation over time. For longer sequences, this process can be repeated, with the interpolation model generating seamless transitions between segments. In addition to generating realistic, long-term animations, our pipeline allows for emotions that evolve over time, leveraging the keyframe generation model’s broad contextual span.

Our main contributions can be summarized as follows:

- **State-of-the-art long-term animation:** We introduce a state-of-the-art method that combines keyframe generation with interpolation to produce videos that maintain high quality over time and capture long-range temporal dependencies.
- **Continuous emotion modelling:** Using valence and arousal, we enhance the emotional expressiveness of facial animations, allowing for nuanced portrayals of gradual emotional transitions.
- **Integration of non-speech vocalizations:** We extend the communicative capabilities of our model by incorporating NSVs for more natural animations.

2. Related Works

Audio-driven facial animation Audio-driven facial animation methods [30, 58, 75] generate realistic talking-head sequences with audio-synchronized lip movements. Early models, such as [58], used GANs, introducing a temporal GAN to generate talking-head videos from a still image and

audio input, while Wav2Lip [46] improved lip-sync accuracy with a pre-trained expert discriminator. More recent 3D-aware and head pose-driven methods [7, 75, 77] aimed to capture head motion, though often struggled with artefacts and unnatural movements.

In contrast to GANs, which face challenges like mode collapse [1], DMs excel in conditional image and video generation [47, 73] and are promising for facial animation [15, 66]. In [52], an autoregressive diffusion model generates head motions and expressions from audio but face challenges with long-term consistency. Recent methods [11, 59, 65] use video DMs [3, 23] for improved temporal coherence. For instance, AniPortrait [63] conditions on audio-predicted facial landmarks, but converting audio to latent motion (e.g., landmarks [63] or 3D meshes [71]) remains challenging, often yielding synthetic-looking motion. Similarly, [66] proposes a two-stage approach that disentangles motion and identity, but assumes strict separation, which is not always respected. To preserve identity across generated frames, several methods [11, 59, 63] leverage ReferenceNet [24], which provides identity information, but increases resource demands. In contrast, KeyFace addresses these limitations by combining keyframe prediction and interpolation for temporally coherent, identity-preserving animations without relying on intermediate representations or ReferenceNet. Although similar approaches have been applied to video generation [3, 51] and controllable animation [42], ours is the first to apply this method to audio-driven animation.

Emotion-driven generation Controllable emotion has recently become a key focus in audio-driven facial animation to create more realistic, empathetic avatars. Most works [10, 17, 19, 38] use discrete emotion labels (e.g. angry or sad) with intensity levels, but this approach lacks expressivity beyond predefined classes. Some approaches use a driving video or audio as a richer emotional source [27, 36, 44, 49, 55], generating a latent representation from the media to drive the animation. This latent representation can sometimes be interpolated to control the resulting emotion [26]. However, they require the driving audio or video during inference, limiting expressiveness and restricting explicit control. Continuous emotion conditioning, using valence and arousal, remains underexplored, despite evidence that it better captures emotional complexity [2, 62]. Additionally, few works allow for continuous emotion variation within a video, and those that do are often limited to a small set of emotions [64], likely due to challenges in achieving coherent long-term animation.

Non-speech vocalizations Non-speech vocalizations (NSVs), such as laughter and sighs, significantly enhance human communication [45, 48] by providing context

beyond words and increasing speech naturalness. Despite this, NSVs are often overlooked in audio-driven facial animation, and state-of-the-art models trained only on speech typically perform poorly on NSVs. Recently, two models have aimed to address this gap: Laughing Matters [5], which proposes a diffusion model that can produce realistic laughter videos from still images and audio, and LaughTalk [54], a 3D model that generates both speech and laughter. However, a model capable of handling multiple NSVs in addition to speech has not yet been explored.

3. Method

Our two-stage approach, outlined in Fig. 2, starts with the generation of temporally distant keyframes. In the second stage, an interpolation model animates the full sequence by filling gaps between the generated keyframes. Our architecture builds upon Stable Video Diffusion (SVD) [3], with further architectural details and key distinctions provided in Appendix B.

3.1. Latent diffusion

Diffusion models [13, 22] are generative models structured as Markov chains with a Gaussian kernel, consisting of two main processes. The forward process gradually adds noise to the initial data point, while the reverse process denoises samples in multiple steps. Traditional diffusion models require many sampling steps to achieve high-quality images, which can be computationally demanding. The EDM framework [31], which defines the diffusion process as a stochastic differential equation and employs an Euler solver for denoising, reduces the necessary diffusion steps by parametrising the learnable denoiser D_θ as

$$D_\theta(\mathbf{x}; \sigma) = c_{\text{skip}}(\sigma)\mathbf{x} + c_{\text{out}}(\sigma)F_\theta(c_{\text{in}}(\sigma)\mathbf{x}; c_{\text{noise}}(\sigma)), \quad (1)$$

where F_θ is the network to be trained, \mathbf{x} is the model input, and c_{noise} , c_{out} , c_{skip} , and c_{in} are scaling factors that depend on the noise level σ . Latent Diffusion Models (LDMs) [47] further reduce computational demands by integrating a pre-trained Variational Autoencoder (VAE) [35]. Rather than operating in the original high-dimensional space, LDMs map data into a compact latent space via an encoder, where diffusion is applied more efficiently. The latent samples are subsequently decoded back to the original space.

3.2. Keyframe generation

In the first stage, we generate keyframes that capture essential facial expressions and movements, guided by the audio over an extended temporal context. These keyframes act as anchor points for the subsequent interpolation stage, ensuring that the final animation accurately reflects both the audio content and the associated emotional expressions. We

generate T keyframes, spaced S frames apart, to capture long-range temporal dependencies efficiently.

Given a noised input sequence $z_k \in \mathbb{R}^{C \times T \times H \times W}$, where C is the number of channels, and $H \times W$ are the spatial dimensions, our goal is to generate a sequence of a person speaking in sync with the given audio. To provide identity and background information, we repeat an identity frame $x_{id} \in \mathbb{R}^{C \times H \times W}$, pass it through the VAE encoder, and concatenate it with the noised input, effectively leveraging the U-Net architecture’s skip connections to preserve input details. Additionally, the model is conditioned on audio embeddings (see Section 3.4), along with emotional valence and arousal (see Section 3.5).

3.3. Interpolation

After generating the main frames that capture essential facial expressions and movements, the next step is to interpolate between these keyframes to produce a smooth and coherent video sequence.

We use the same architecture as the keyframe model, adapted for the interpolation task. We take two consecutive frames z_s and z_e from the keyframe sequence as conditioning frames. To match the input shape $z_i \in \mathbb{R}^{C \times S \times H \times W}$, we create a sequence

$$s = \{z_s, \underbrace{z_m, \dots, z_m}_{\text{repeat } S-2 \text{ times}}, z_e\} \in \mathbb{R}^{C \times S \times H \times W},$$

where $z_m \in \mathbb{R}^{C \times H \times W}$ is a learned embedding that represents the missing frames. This sequence is concatenated channel-wise with the noise input. We also incorporate a binary mask $M \in \mathbb{R}^{S \times 1 \times H \times W}$, where $M_s = 1$ if s corresponds to a conditioning frame ($s = 1$ or $s = T$), and $M_s = 0$ otherwise. This mask helps the model distinguish between conditioned and unconditioned frames, allowing it to focus on interpolating the intermediate frames.

3.4. Audio encoding

For audio processing, we combine embeddings from two pre-trained audio encoders: WavLM $A_w \in \mathbb{R}^{L \times C^a}$ [8], which excels at capturing linguistic content from speech, and BEATs $A_b \in \mathbb{R}^{L \times C^a}$ [9], which is trained to extract features from a broader range of acoustic signals, including non-speech sounds. We define $L \in \{T, S\}$ based on whether we use the interpolation or keyframe model and C^a as the audio embedding dimension. By concatenating these embeddings, we obtain $A_{wb} = \text{Concat}(A_w, A_b) \in \mathbb{R}^{L \times 2C^a}$, which we feed to the model via two mechanisms:

- **Audio Attention Blocks:** The combined embeddings serve as keys and values in the cross-attention layers within the U-Net, enabling the model to attend to relevant audio features.
- **Timestep Embeddings:** We pass A_{wb} through an MLP and add it to the diffusion timestep embeddings $t_s \in \mathbb{R}^{C^s}$,

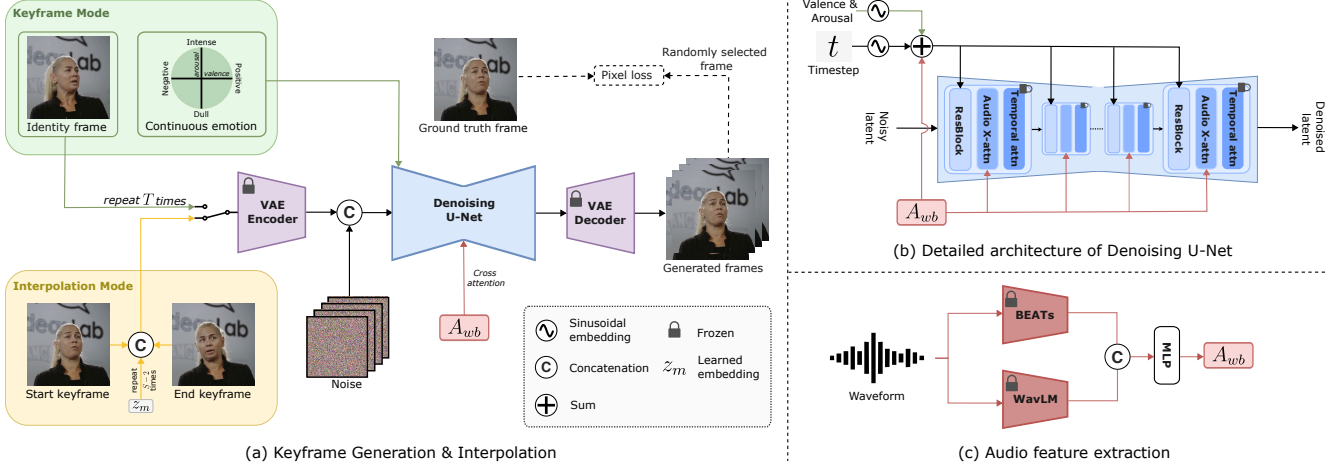


Figure 2. Overview of KeyFace’s two-stage framework. The main architecture (a) is shared between the two stages, differing only in the conditioning inputs. A detailed view is provided in (b). In the keyframe generation stage, the model receives an identity frame x_{id} , repeated and concatenated with the noised video input to match the input dimensions. In the interpolation stage, the model is conditioned on two consecutive frames z_s and z_e from the keyframe sequence, interpolating the intermediate frames using a learned masked embedding z_m and a binary mask M . Both stages incorporate audio embeddings A_{wb} from WavLM and BEATs (c). We also use continuous emotion embeddings in the keyframe generation that accurately convey both speech content and emotional expressions.

yielding $t'_s = t_s + \text{MLP}(A_{\text{wb}})$, where C^s is the timestep embedding dimension. This encourages alignment between image and audio frames.

3.5. Emotion modelling with valence and arousal

To capture complex, continuously changing emotional expressions, we adopt a continuous representation based on valence and arousal. For each frame, we extract valence and arousal using a pre-trained emotion recognition model [50], encode them into sinusoidal embeddings $E_v, E_a \in \mathbb{R}^{C^s}$, and add them to the diffusion timestep embedding along with the audio embeddings:

$$t''_s = t'_s + E_v + E_a. \quad (2)$$

Notably, we find that incorporating emotions solely in the keyframe model is sufficient for achieving effective emotional control, as the interpolation model can propagate emotional expressions without additional conditioning. During inference, users can provide any valence and arousal to guide the generation of desired emotional states.

3.6. Losses

Working in latent space is computationally efficient, but due to the compressed representations, it can be challenging for the model to retain fine semantic details from the original image [72]. This issue is particularly critical for faces, as humans are highly sensitive to minor imperfections in facial features, which can disrupt the perceived realism and emotional expressiveness of animations. To mitigate this, we decode the latent sequence z_0 back to RGB space to ob-

tain $x_0 \in \mathbb{R}^{3 \times L \times H \times W}$. We then apply an L_2 loss between the decoded frames x_0 and the ground truth frames x_{gt} , and add it to the existing L_2 loss between the latent representations z_0 and z_{gt} . We also include a perceptual loss L_p based on features extracted from a pre-trained VGG network [29], which encourages the generated images to be perceptually similar to the ground truth, enhancing visual quality.

To reduce memory consumption, we apply the additional pixel losses to a single random frame rather than the entire sequence, which proves sufficient for producing high-quality results. In contrast, the standard diffusion loss continues to be applied across all frames. Moreover, we introduce a specialized weight λ_{lower} applied to the lower half of the image, which helps the model focus on the mouth region. This spatially targeted weight, within the compressed latent space, enhances lip synchronization quality by emphasizing the alignment between generated lip movements and audio inputs, which is crucial for realistic audio-driven animations. The total loss function is defined as

$$L = \lambda_{\text{tot}} (L_2(z_0, z_{\text{gt}}) + L_2(x_0, x_{\text{gt}}) + L_p(x_0, x_{\text{gt}})), \quad (3)$$

where $\lambda_{\text{tot}} = \lambda(t)\lambda_{\text{lower}}$ and $\lambda(t)$ is a weighting factor that depends on the diffusion timestep t , as defined in [31].

3.7. Guidance

For the keyframe model, we use a modified version of classifier-free guidance (CFG) [21], split into two parts: one for audio control and the other for identity control, allowing separate scales for each. The guidance formula is

$$z = z_{\emptyset} + w_{\text{id}} \cdot (z_{\text{id}} - z_{\emptyset}) + w_{\text{aud}} \cdot (z_{\text{id} \& \text{aud}} - z_{\text{id}}), \quad (4)$$

where w_{aud} and w_{id} are the guidance scales for audio and identity, respectively. Here, z_\emptyset is the model output with all conditions set to 0, z_{id} is the output with only the identity condition, and $z_{\text{id} \& \text{aud}}$ is the output with both conditions.

While CFG is effective in many scenarios, it can overly amplify the conditioning signal, reducing output diversity [32]. In the interpolation stage, where subtle emotional expressions and fluid motion are critical, CFG may be ill-suited. Autoguidance [32], addresses this by using a model that is either smaller or trained with fewer steps to guide the main diffusion process, balancing guidance for improved video quality without sacrificing diversity. Autoguidance is formulated as

$$D(x; \sigma, c) = D_r(\cdot) + w_{\text{auto}} \cdot (D_m(\cdot) - D_r(\cdot)), \quad (5)$$

where $D(x; \sigma, c)$ is the guided denoising step, $D_r(\cdot)$ is the reduced model, $D_m(\cdot)$ is the fully trained guiding model, and w_{auto} controls the guiding model's influence.

4. Experiments

4.1. Datasets

We train both models on HDTF [76] and a dataset that we collected, comprising 160 hours of speech and 30 hours of NSVs. We also experiment with CelebV-Text [70] and CelebV-HQ [78] but find that excluding these lower-quality datasets benefits training. For testing, we use the HDTF test set, and 100 videos randomly selected from CelebV-Text. Additionally, to evaluate our emotion control, we use a test set selected from MEAD [60], as in [55].

4.2. Evaluation metrics

We evaluate image quality using the aesthetic quality metric from V-Bench [25], Fréchet Inception Distance (FID) [20], and Learned Perceptual Image Patch Similarity (LPIPS) [74]. For general video quality, we use Fréchet Video Distance (FVD) [57] and the smoothness metric from [25]. We compute the emotion accuracy (Emo_{acc}) using the pre-trained emotion recognition model from [50]. We also introduce two new metrics, further details are provided in Appendix D.

LipScore. The typical metric for audio-visual synchronization, SyncNet [46], has known limitations, including low correlation with lip-sync quality and significant reliability issues even on ground truth data [14, 19, 68]. To address this, we introduce a lipreading perceptual score (LipScore) inspired by [6], which computes the cosine similarity between the generated and ground truth embeddings extracted from the final layer of a state-of-the-art lipreader [41]. This lipreader is trained on 6× more data than SyncNet, providing higher-quality embeddings that better correlate with human perception.

NSV accuracy. To evaluate the model's ability to generate NSVs, we train a video classifier to recognize 8 NSV types ("Mhm", "Oh", "Ah", coughs, sighs, yawns, throat clears, and laughter) plus speech, for a total of 9 classes. The classifier is based on a pre-trained MViT2 [37] for video classification on the Kinetics dataset [33]. We then employ it to evaluate the model's ability to generate the correct NSV type and measure the overall accuracy, denoting this metric as NSV accuracy (NSV_{acc}).

4.3. User study

To provide a more comprehensive evaluation, we conduct a user study inspired by [12]. We select 20 videos per model (see Table 1) and present participants with pairs of 5-second videos featuring the same audio and identity, asking them to choose the more realistic video based on visual quality, lip synchronization, and motion realism. We surveyed 51 participants, each of whom compared an average of 20 video pairs. We use an Elo rating system [16] with bootstrapping applied to obtain a more stable ranking [12].

5. Results

This section presents a comprehensive evaluation of our model, including comparisons with established methods and ablation studies to assess the impact of key components.

5.1. Quantitative analysis

We present a quantitative comparison against current state-of-the-art methods in Table 1. KeyFace achieves the lowest FID and FVD, indicating higher realism and temporal coherence. Our model also achieves the highest AQ and LPIPS, confirming the visual appeal of our animations. While SadTalker and V-Express achieve the highest smoothness and LipScores, respectively, KeyFace ranks a close second and outperforms both SadTalker and V-Express on the other metrics, demonstrating better performance overall. Figure 3 illustrates FID over time for videos generated by each method, where our two-stage approach maintains consistent quality without degradation. In contrast, Hallo and AniPortrait suffer from significant quality loss over time. To ensure fairness in evaluation, we also report results for a variant of our model trained exclusively on HDTF in Appendix F.

Additionally, the user study results (Elo) show that our model is preferred over other methods, confirming the effectiveness of our approach. A detailed analysis of the results is provided in Appendix E.

5.2. Emotional results

To assess our model's ability to generate accurate emotional expressions, we evaluate it on MEAD [60], comparing it to state-of-the-art models in Table 2.

Method	AQ \uparrow	FID \downarrow	LPIPS \downarrow	FVD \downarrow	Smoothness \uparrow	LipScore \uparrow	Elo \uparrow	
HDTF	SadTalker [75]	0.52	60.55	0.44	410.86	0.9955	0.24	960.44
	Haloo [65]	0.55	<u>19.22</u>	<u>0.17</u>	236.97	0.9939	0.27	1054.69
	V-Express [59]	0.55	34.68	0.21	<u>200.67</u>	0.9943	0.37	985.35
	AniPortrait [63]	<u>0.56</u>	20.68	0.19	299.09	0.9951	0.14	887.84
	EchoMimic [11]	0.55	20.35	0.18	213.30	0.9928	0.17	1023.53
CelebV-Text	KeyFace	0.59	16.76	0.16	137.25	<u>0.9952</u>	<u>0.36</u>	1091.52
	SadTalker [75]	0.49	49.85	0.49	434.31	0.9959	0.25	950.56
	Haloo [65]	0.50	24.86	0.27	310.00	0.9938	0.29	1020.27
	V-Express [59]	0.51	26.46	<u>0.22</u>	<u>253.16</u>	0.9933	0.32	<u>1044.43</u>
	AniPortrait [63]	<u>0.52</u>	24.84	0.28	373.32	0.9950	0.12	841.79
	EchoMimic [11]	0.51	<u>22.81</u>	0.26	298.33	0.9921	0.18	1043.26
KeyFace	KeyFace	0.55	17.06	0.21	180.26	<u>0.9952</u>	<u>0.30</u>	1100.90

Table 1. **Quantitative comparisons** on HDTF [76] and CelebV-Text [70] between our model and state-of-the-art facial animation methods. The best results are highlighted in **bold**, and the second-best results are underlined. All the metrics are described in Section 4.2

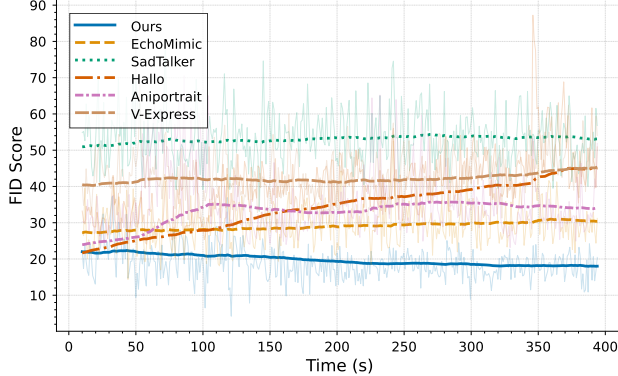


Figure 3. We present sliding window FID with a 1-second window size for videos generated by different methods.

Notably, despite being trained with only pseudo-labels extracted from our training data, KeyFace achieves competitive emotion accuracy compared to other models, which are trained on ground-truth labels from MEAD, outperforming 2 out of 3 models while delivering significantly better image and video quality. We also show that using continuous emotion labels (valence and arousal) yields significant improvements compared to discrete labels, and allows our model to generate multiple emotions within a single video by interpolating between points in the valence and arousal space, as illustrated in Figure 4.

5.3. Ablation Studies

Audio Encoder. We evaluate the impact of different audio encoders on the model’s ability to handle both speech and non-speech vocalizations (NSVs). As shown in Table 3, the combination of WavLM and BEATs achieves the best over-

Method	Emotion Source	FID \downarrow	FVD \downarrow	Emo _{acc} \uparrow
EDTalk [55]	Video	101.19	619.90	0.72
EAT [17]	Discrete Labels	75.69	560.61	0.54
EAMM [27]	Video	107.16	855.20	0.17
KeyFace	Discrete Labels	<u>50.34</u>	<u>509.13</u>	0.43
KeyFace	Valence & arousal	44.43	447.74	<u>0.67</u>

Table 2. **Emotion evaluation** on MEAD [60]. Default settings are highlighted in **gray** on all tables.

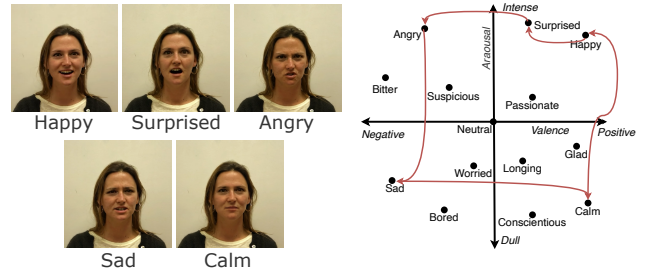


Figure 4. We show KeyFace’s ability to interpolate between several different emotions within the same video.

all performance. BEATs is shown to significantly improve the handling of NSV, aligning with the findings of [5]. Likewise, when it is removed, the ability to generate the correct NSVs becomes close to random probability. Finally, WavLM improves lip synchronization quality compared to Wav2Vec2, with only a slight sacrifice in image quality, as indicated by a marginal increase in FID.

Architecture. We assess two key architectural modifications in Table 4. First, we examine the effect of removing temporal layers for keyframe generation, which leads

Audio backbone	FID ↓	FVD ↓	LipScore ↑	NSV_{acc} ↑
WavLM	16.89	147.12	0.36	0.10
BEATs	19.52	212.47	0.29	0.23
Wav2vec2 + BEATs	16.00	<u>143.97</u>	<u>0.32</u>	<u>0.31</u>
WavLM + BEATs	<u>16.76</u>	137.25	0.36	0.42

Table 3. **Audio encoder ablation** on HDTF [76]. For NSV_{acc} , we use HDTF identities with audio containing NSVs.

to overly static frames, highlighting the importance of generating keyframes as a cohesive sequence. Second, we replace the concatenation operation with ReferenceNet, inspired by recent trends from [24], and find that it requires twice as many training steps to achieve acceptable results. Even then, it results in lower video quality, introducing inconsistencies in background continuity and face shape.

Method	FID ↓	FVD ↓	LipScore ↑
w/o temporal layers	<u>23.74</u>	<u>250.30</u>	0.25
w/o Concat, w/ Reference Net	39.71	401.70	<u>0.32</u>
Concat w/ temporal layers	16.76	137.25	0.36

Table 4. **Architecture ablation** on HDTF [76].

Losses. We compare the effects of different pixel loss functions and weights in Table 5. First, we see that having a pixel-space loss proves to be beneficial regardless of the loss type. The L1 loss yields improved image quality and lip synchronisation, but restricts model flexibility compared to the L2 loss, resulting in a higher FVD. In addition, incorporating the L_p loss noticeably improves visual quality for both losses, as shown by the decreased FID. Overall, combining L_2 and L_p losses produces the best balance of quality, variety, and lip synchronisation. Next, we examine λ_{lower} , which controls the weight of the pixel loss for the lower part of the video. Choosing a higher weight improves animation quality and lip synchronization, but increasing it too much overemphasizes this region and reduces overall quality. A good balance is achieved with $\lambda_{lower} = 3$.

Data. We test the effect of adding additional training data to each stage in Table 6. Both models experience a decline in performance when trained with data of lower quality, confirming our hypothesis from Section 4.1. We find that training exclusively on high-quality data primarily improves lip synchronization for the interpolation model, while conversely enhancing video quality for the keyframe model, as indicated by lower FID and FVD scores, respectively. This suggests that each model plays a distinct role in the generation process and therefore reacts differently to changes in training data.

Method	FID ↓	FVD ↓	LipScore ↑
No pixel loss	18.76	148.22	0.33
L_1 only	17.66	172.01	0.37
L_2 only	19.00	<u>137.54</u>	0.34
$L_1 + L_p$	<u>17.02</u>	169.01	0.34
$L_2 + L_p$	16.76	137.25	<u>0.36</u>
$\lambda_{lower} = 1$	17.40	186.87	0.33
$\lambda_{lower} = 2$	16.71	<u>147.01</u>	<u>0.35</u>
$\lambda_{lower} = 3$	<u>16.76</u>	137.25	0.36
$\lambda_{lower} = 4$	17.36	161.40	<u>0.35</u>

Table 5. **Loss ablation** on HDTF [76].

Training set	Keyframe	Interpolation	FID ↓	FVD ↓	LipScore ↑
All	All		26.92	253.24	0.24
All	HQ only		24.45	236.75	<u>0.31</u>
HQ only	All		<u>16.97</u>	<u>166.81</u>	0.24
HQ only	HQ only		16.76	137.25	0.36

Table 6. **Data Ablation** on HDTF [76]. “HQ only” refers to our high quality training set (HDTF and collected data), while “All” refers to all training data, including CelebV-Text and CelebV-HQ.

Guidance. We compare different guidance types in Table 7. Using CFG for both models makes videos overly static, as it closely adheres to the keyframes, limiting expression range and animation flow, as shown by the lower FVD. In contrast, applying autoguidance to the keyframe model worsens alignment with audio, resulting in lower LipScores. Using CFG instead allows for a separate grid searches for audio and identity guidance scales (Fig. 5), increasing flexibility and enhancing model performance.

Guidance method		FID ↓	FVD ↓	LipScore ↑
Keyframe	Interpolation			
Autoguidance [32]	CFG [21]	20.12	172.31	0.31
Autoguidance [32]	Autoguidance [32]	18.86	<u>152.77</u>	<u>0.33</u>
CFG [21]	CFG [21]	<u>18.53</u>	177.09	0.32
CFG [21]	Autoguidance [32]	16.76	137.25	0.36

Table 7. **Guidance Ablation** on HDTF [76].

5.4. Qualitative analysis

Motion. We compare the motion generated by KeyFace to that of other existing models by analysing the average optical flow magnitude in the predicted videos in Fig. 6. AniPortrait and V-Express are excluded from this analysis, as they are conditioned on the ground-truth motion and therefore are not suitable for a fair comparison. We see that models like Hallo and EchoMimic, which rely on ReferenceNet,

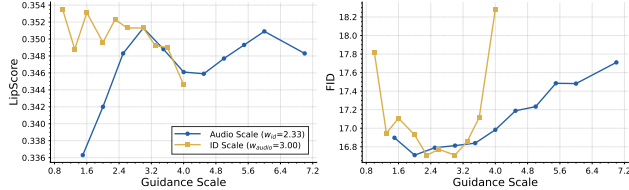


Figure 5. We show the impact of **guidance scale** for identity and audio condition on FID and LipScore on HDTF [76].

tend to produce background inconsistencies over time, as shown by the noisy patterns surrounding the speaker’s silhouette, while SadTalker generates relatively static videos of lower quality, as indicated by a sparser optical flow map. In contrast, we find that KeyFace generates motion patterns that more closely align with those observed in real videos, outperforming other methods.

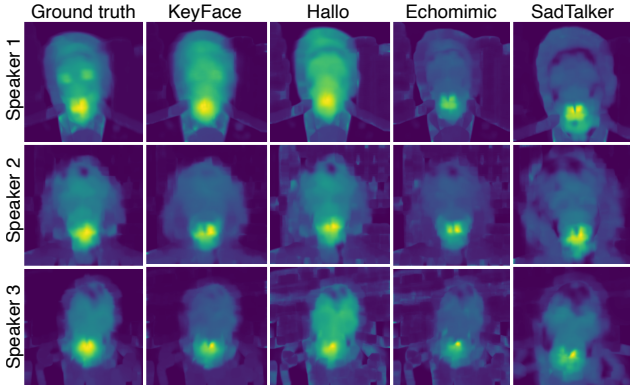


Figure 6. We show the average optical flow magnitude accross different speakers and models.

Visual Quality. Figure 8 compares our model with other methods on the same audio input using an out-of-distribution identity frame, revealing key limitations in existing approaches. AniPortrait and SadTalker exhibit repetitive movements, V-Express treats hair accessories as background, causing unnatural head movements around the accessory, and EchoMimic introduces inconsistent head movements and background artifacts across frames. Hallo, on the other hand, produces natural motion, but suffers from error accumulation. Finally, KeyFace produces natural and varied head motion while achieving the best lip synchronization, on par with V-Express. We highlight our model’s ability to accurately animate non-speech vocalizations in Figure 7, emphasizing our holistic approach to facial animation compared to existing methods that can only handle speech. For a more comprehensive evaluation, we strongly encourage readers to refer to the supplementary material.



Figure 7. Examples of different NSVs generated using KeyFace, highlighting the model’s capability to handle non-speech audio.

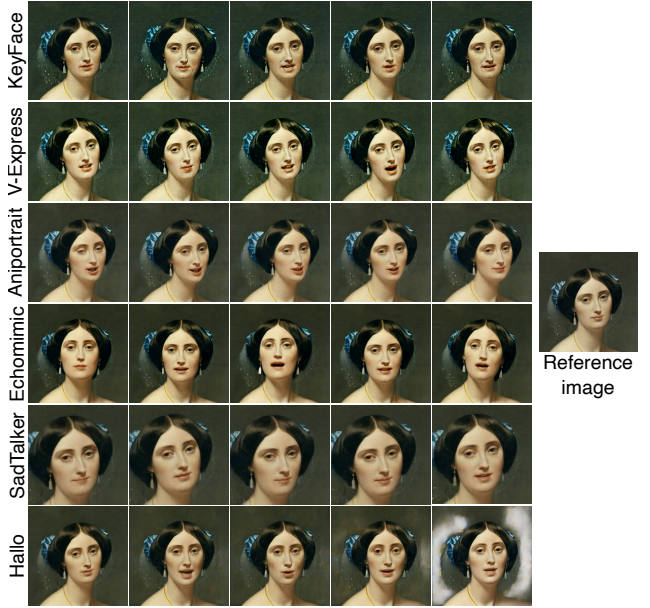


Figure 8. Results on out-of-distribution id using the same audio. Please refer to our project page for additional video comparisons.

6. Conclusion

We introduce **KeyFace**, a two-stage diffusion-based framework for generating long-duration, coherent, and natural audio-driven facial animations. By leveraging an extended temporal context through keyframe generation and interpolation, our method effectively preserves temporal coherence and realism across long sequences. We further increase the expressiveness of facial animations by conditioning on continuous emotions for long-term emotional control, and adding NSVs to our training set. Experimental results demonstrate that KeyFace outperforms state-of-the-art methods across a comprehensive set of objective metrics. Finally, we consolidate our findings via a series of qualitative evaluations and prove that KeyFace successfully addresses key challenges such as repetitive movements and error accumulation, setting a new standard for natural and expressive animations over long durations.

References

- [1] Martín Arjovsky, Soumith Chintala, and Léon Bottou. Wasserstein generative adversarial networks. In *Proceedings of the 34th International Conference on Machine Learning, ICML 2017, Sydney, NSW, Australia, 6-11 August 2017*, pages 214–223. PMLR, 2017. 2
- [2] Sinem Aslan, Eda Okur, Nese Alyüz, Asli Arslan Esme, and Ryan S. Baker. Towards human affect modeling: A comparative analysis of discrete affect and valence-arousal labeling. In *HCI International 2018 - Posters' Extended Abstracts - 20th International Conference, HCI International 2018, Las Vegas, NV, USA, July 15-20, 2018, Proceedings, Part II*, pages 372–379. Springer, 2018. 2
- [3] Andreas Blattmann, Tim Dockhorn, Sumith Kulal, Daniel Mendelevitch, Maciej Kilian, Dominik Lorenz, Yam Levi, Zion English, Vikram Voleti, Adam Letts, Varun Jampani, and Robin Rombach. Stable video diffusion: Scaling latent video diffusion models to large datasets, 2023. 2, 3, 1
- [4] Andreas Blattmann, Robin Rombach, Huan Ling, Tim Dockhorn, Seung Wook Kim, Sanja Fidler, and Karsten Kreis. Align your latents: High-resolution video synthesis with latent diffusion models. In *IEEE Conference on Computer Vision and Pattern Recognition (CVPR)*, 2023. 1
- [5] Antoni Bigata Casademunt, Rodrigo Mira, Nikita Drobyshev, Konstantinos Vougioukas, Stavros Petridis, and Maja Pantic. Laughing matters: Introducing laughing-face generation using diffusion models. *arXiv preprint arXiv:2305.08854*, 2023. 3, 6
- [6] Lele Chen, Guofeng Cui, Ziyi Kou, Haitian Zheng, and Chenliang Xu. What comprises a good talking-head video generation?: A survey and benchmark. *CoRR*, abs/2005.03201, 2020. 5
- [7] Lele Chen, Guofeng Cui, Celong Liu, Zhong Li, Ziyi Kou, Yi Xu, and Chenliang Xu. Talking-head generation with rhythmic head motion. In *European Conference on Computer Vision*, pages 35–51. Springer, 2020. 2
- [8] Sanyuan Chen, Chengyi Wang, Zhengyang Chen, Yu Wu, Shujie Liu, Zhuo Chen, Jinyu Li, Naoyuki Kanda, Takuya Yoshioka, Xiong Xiao, Jian Wu, Long Zhou, Shuo Ren, Yanmin Qian, Yao Qian, Jian Wu, Michael Zeng, Xiangzhan Yu, and Furu Wei. Wavlm: Large-scale self-supervised pre-training for full stack speech processing. *IEEE J. Sel. Top. Signal Process.*, 16(6):1505–1518, 2022. 3, 1
- [9] Sanyuan Chen, Yu Wu, Chengyi Wang, Shujie Liu, Daniel Tompkins, Zhuo Chen, Wanxiang Che, Xiangzhan Yu, and Furu Wei. Beats: Audio pre-training with acoustic tokenizers. In *International Conference on Machine Learning, ICML 2023, 23-29 July 2023, Honolulu, Hawaii, USA*, pages 5178–5193. PMLR, 2023. 3, 1
- [10] Yutong Chen, Junhong Zhao, and Wei-Qiang Zhang. Expressive speech-driven facial animation with controllable emotions. In *2023 IEEE International Conference on Multimedia and Expo Workshops (ICMEW)*, pages 387–392. IEEE, 2023. 2
- [11] Zhiyuan Chen, Jiajiong Cao, Zhiqian Chen, Yuming Li, and Chenguang Ma. Echomimic: Lifelike audio-driven portrait animations through editable landmark conditions, 2024. 1, 2, 6
- [12] Wei-Lin Chiang, Lianmin Zheng, Ying Sheng, Anastasios Nikolas Angelopoulos, Tianle Li, Dacheng Li, Hao Zhang, Banghua Zhu, Michael Jordan, Joseph E. Gonzalez, and Ion Stoica. Chatbot arena: An open platform for evaluating llms by human preference, 2024. 5
- [13] Prafulla Dhariwal and Alexander Quinn Nichol. Diffusion models beat gans on image synthesis. In *Advances in Neural Information Processing Systems 34: Annual Conference on Neural Information Processing Systems 2021, NeurIPS 2021, December 6-14, 2021, virtual*, pages 8780–8794, 2021. 1, 3
- [14] Nikita Drobyshev, Antoni Bigata Casademunt, Konstantinos Vougioukas, Zoe Landgraf, Stavros Petridis, and Maja Pantic. Emoportraits: Emotion-enhanced multimodal one-shot head avatars. In *IEEE/CVF Conference on Computer Vision and Pattern Recognition, CVPR 2024, Seattle, WA, USA, June 16-22, 2024*, pages 8498–8507. IEEE, 2024. 5, 2
- [15] Chenpeng Du, Qi Chen, Tianyu He, Xu Tan, Xie Chen, Kai Yu, Sheng Zhao, and Jiang Bian. Dae-talker: High fidelity speech-driven talking face generation with diffusion autoencoder. In *Proceedings of the 31st ACM International Conference on Multimedia*, pages 4281–4289, 2023. 2
- [16] Arpad E. Elo. *The Rating of Chessplayers, Past and Present*. Arco Pub., New York, 1978. 5
- [17] Yuan Gan, Zongxin Yang, Xihang Yue, Lingyun Sun, and Yi Yang. Efficient emotional adaptation for audio-driven talking-head generation. In *Proceedings of the IEEE/CVF International Conference on Computer Vision (ICCV)*, pages 22634–22645, 2023. 2, 6
- [18] Ian J. Goodfellow, Jean Pouget-Abadie, Mehdi Mirza, Bing Xu, David Warde-Farley, Sherjil Ozair, Aaron C. Courville, and Yoshua Bengio. Generative adversarial networks. *Commun. ACM*, 63(11):139–144, 2020. 1
- [19] Siddharth Gururani, Arun Mallya, Ting-Chun Wang, Rafael Valle, and Ming-Yu Liu. Space: Speech-driven portrait animation with controllable expression. In *Proceedings of the IEEE/CVF International Conference on Computer Vision*, pages 20914–20923, 2023. 2, 5
- [20] Martin Heusel, Hubert Ramsauer, Thomas Unterthiner, Bernhard Nessler, and Sepp Hochreiter. Gans trained by a two time-scale update rule converge to a local nash equilibrium. In *Advances in Neural Information Processing Systems 30: Annual Conference on Neural Information Processing Systems 2017, December 4-9, 2017, Long Beach, CA, USA*, pages 6626–6637, 2017. 5
- [21] Jonathan Ho and Tim Salimans. Classifier-free diffusion guidance, 2022. 4, 7, 1
- [22] Jonathan Ho, Ajay Jain, and Pieter Abbeel. Denoising diffusion probabilistic models. In *Advances in Neural Information Processing Systems 33: Annual Conference on Neural Information Processing Systems 2020, NeurIPS 2020, December 6-12, 2020, virtual*, 2020. 1, 3
- [23] Jonathan Ho, Tim Salimans, Alexey Gritsenko, William Chan, Mohammad Norouzi, and David J Fleet. Video diffusion models. *Advances in Neural Information Processing Systems*, 35:8633–8646, 2022. 2

- [24] Li Hu. Animate anyone: Consistent and controllable image-to-video synthesis for character animation. In *IEEE/CVF Conference on Computer Vision and Pattern Recognition, CVPR 2024, Seattle, WA, USA, June 16-22, 2024*, pages 8153–8163. IEEE, 2024. 2, 7
- [25] Ziqi Huang, Yinan He, Jiahuo Yu, Fan Zhang, Chenyang Si, Yuming Jiang, Yuanhan Zhang, Tianxing Wu, Qingyang Jin, Nattapol Chanpaisit, Yaohui Wang, Xinyuan Chen, Limin Wang, Dahua Lin, Yu Qiao, and Ziwei Liu. Vbench: Comprehensive benchmark suite for video generative models. In *IEEE/CVF Conference on Computer Vision and Pattern Recognition, CVPR 2024, Seattle, WA, USA, June 16-22, 2024*, pages 21807–21818. IEEE, 2024. 5
- [26] Xinya Ji, Hang Zhou, Kaisiyuan Wang, Wayne Wu, Chen Change Loy, Xun Cao, and Feng Xu. Audio-driven emotional video portraits. In *IEEE Conference on Computer Vision and Pattern Recognition, CVPR 2021, virtual, June 19-25, 2021*, pages 14080–14089. Computer Vision Foundation / IEEE, 2021. 2
- [27] Xinya Ji, Hang Zhou, Kaisiyuan Wang, Qianyi Wu, Wayne Wu, Feng Xu, and Xun Cao. Eamm: One-shot emotional talking face via audio-based emotion-aware motion model. In *ACM SIGGRAPH 2022 Conference Proceedings*, pages 1–10, 2022. 2, 6
- [28] Esperanza Johnson, Ramón Hervás, Carlos Gutiérrez López de la Franca, Tania Mondéjar, Sergio F Ochoa, and Jesús Favela. Assessing empathy and managing emotions through interactions with an affective avatar. *Health informatics journal*, 24(2):182–193, 2018. 1
- [29] Justin Johnson, Alexandre Alahi, and Li Fei-Fei. Perceptual losses for real-time style transfer and super-resolution. In *Computer Vision - ECCV 2016 - 14th European Conference, Amsterdam, The Netherlands, October 11-14, 2016, Proceedings, Part II*, pages 694–711. Springer, 2016. 4
- [30] Tero Karras, Timo Aila, Samuli Laine, Antti Herva, and Jaakko Lehtinen. Audio-driven facial animation by joint end-to-end learning of pose and emotion. *ACM Transactions on Graphics (ToG)*, 36(4):1–12, 2017. 2
- [31] Tero Karras, Miika Aittala, Timo Aila, and Samuli Laine. Elucidating the design space of diffusion-based generative models. In *Advances in Neural Information Processing Systems 35: Annual Conference on Neural Information Processing Systems 2022, NeurIPS 2022, New Orleans, LA, USA, November 28 - December 9, 2022*, 2022. 3, 4, 1
- [32] Tero Karras, Miika Aittala, Tuomas Kynkänniemi, Jaakko Lehtinen, Timo Aila, and Samuli Laine. Guiding a diffusion model with a bad version of itself, 2024. 5, 7, 1, 2
- [33] Will Kay, Joao Carreira, Karen Simonyan, Brian Zhang, Chloe Hillier, Sudheendra Vijayanarasimhan, Fabio Viola, Tim Green, Trevor Back, Paul Natsev, Mustafa Suleyman, and Andrew Zisserman. The kinetics human action video dataset, 2017. 5, 3
- [34] Greg Kessler. Technology and the future of language teaching. *Foreign language annals*, 51(1):205–218, 2018. 1
- [35] Diederik P. Kingma and Max Welling. Auto-encoding variational bayes. In *2nd International Conference on Learning Representations, ICLR 2014, Banff, AB, Canada, April 14-16, 2014, Conference Track Proceedings*, 2014. 3
- [36] Seongmin Lee, Jeonghaeng Lee, Hyewon Song, and Sanghoon Lee. Speech-driven emotional 3d talking face animation using emotional embeddings. In *ICASSP 2024-2024 IEEE International Conference on Acoustics, Speech and Signal Processing (ICASSP)*, pages 7840–7844. IEEE, 2024. 2
- [37] Yanghao Li, Chao-Yuan Wu, Haoqi Fan, Karttikeya Mangalam, Bo Xiong, Jitendra Malik, and Christoph Feichtenhofer. Mvitv2: Improved multiscale vision transformers for classification and detection, 2022. 5, 3
- [38] Borong Liang, Yan Pan, Zhizhi Guo, Hang Zhou, Zhibin Hong, Xiaoguang Han, Junyu Han, Jingtuo Liu, Errui Ding, and Jingdong Wang. Expressive talking head generation with granular audio-visual control. In *Proceedings of the IEEE/CVF Conference on Computer Vision and Pattern Recognition*, pages 3387–3396, 2022. 2
- [39] Junhua Liao, Haihan Duan, Kanghui Feng, Wanbing Zhao, Yanbing Yang, and Liangyin Chen. A light weight model for active speaker detection. In *Proceedings of the IEEE/CVF Conference on Computer Vision and Pattern Recognition (CVPR)*, pages 22932–22941, 2023. 2
- [40] Ilya Loshchilov and Frank Hutter. Decoupled weight decay regularization. In *7th International Conference on Learning Representations, ICLR 2019, New Orleans, LA, USA, May 6-9, 2019*. OpenReview.net, 2019. 1
- [41] Pingchuan Ma, Alexandros Haliassos, Adriana Fernandez-Lopez, Honglie Chen, Stavros Petridis, and Maja Pantic. Auto-avsr: Audio-visual speech recognition with automatic labels. In *ICASSP 2023 - 2023 IEEE International Conference on Acoustics, Speech and Signal Processing (ICASSP)*. IEEE, 2023. 5, 3
- [42] Yue Ma, Hongyu Liu, Hongfa Wang, Heng Pan, Yingqing He, Junkun Yuan, Ailing Zeng, Chengfei Cai, Heung-Yeung Shum, Wei Liu, and Qifeng Chen. Follow-your-emoji: Fine-controllable and expressive freestyle portrait animation, 2024. 2
- [43] Frederic I. Parke. Computer generated animation of faces. In *Proceedings of the ACM annual conference, ACM 1972, Boston, MA, USA, August 1972, Volume 1*, pages 451–457. ACM, 1972. 2
- [44] Ziqiao Peng, Haoyu Wu, Zhenbo Song, Hao Xu, Xiangyu Zhu, Jun He, Hongyan Liu, and Zhaoxin Fan. Emotalk: Speech-driven emotional disentanglement for 3d face animation. In *Proceedings of the IEEE/CVF International Conference on Computer Vision*, pages 20687–20697, 2023. 2
- [45] Alex Pentland. *Honest signals: how they shape our world*. MIT press, 2010. 2
- [46] KR Prajwal, Rudrabha Mukhopadhyay, Vinay P Namboodiri, and CV Jawahar. A lip sync expert is all you need for speech to lip generation in the wild. In *Proceedings of the 28th ACM International Conference on Multimedia*, pages 484–492, 2020. 1, 2, 5
- [47] Robin Rombach, Andreas Blattmann, Dominik Lorenz, Patrick Esser, and Björn Ommer. High-resolution image synthesis with latent diffusion models. In *IEEE/CVF Conference on Computer Vision and Pattern Recognition, CVPR 2022, New Orleans, LA, USA, June 18-24, 2022*, pages 10674–10685. IEEE, 2022. 2, 3

- [48] Willibald Ruch and Paul Ekman. The expressive pattern of laughter. In *Emotions, qualia, and consciousness*, pages 426–443. World Scientific, 2001. 2
- [49] Jack R. Saunders and Vinay P. Namboodiri. READ avatars: Realistic emotion-controllable audio driven avatars. In *34th British Machine Vision Conference 2023, BMVC 2023, Aberdeen, UK, November 20-24, 2023*, pages 216–225. BMVA Press, 2023. 2
- [50] Andrey V Savchenko. Hsemotion: High-speed emotion recognition library. *Software Impacts*, 14:100433, 2022. 4, 5
- [51] Uriel Singer, Adam Polyak, Thomas Hayes, Xi Yin, Jie An, Songyang Zhang, Qiyuan Hu, Harry Yang, Oron Ashual, Oran Gafni, Devi Parikh, Sonal Gupta, and Yaniv Taigman. Make-a-video: Text-to-video generation without text-video data. In *The Eleventh International Conference on Learning Representations, ICLR 2023, Kigali, Rwanda, May 1-5, 2023*. OpenReview.net, 2023. 2
- [52] Michal Stypulkowski, Konstantinos Vougioukas, Sen He, Maciej Zieba, Stavros Petridis, and Maja Pantic. Diffused heads: Diffusion models beat gans on talking-face generation. In *IEEE/CVF Winter Conference on Applications of Computer Vision, WACV 2024, Waikoloa, HI, USA, January 3-8, 2024*, pages 5089–5098. IEEE, 2024. 1, 2
- [53] Shaolin Su, Qingsen Yan, Yu Zhu, Cheng Zhang, Xin Ge, Jinqiu Sun, and Yanning Zhang. Blindly assess image quality in the wild guided by a self-adaptive hyper network. In *IEEE/CVF Conference on Computer Vision and Pattern Recognition (CVPR)*, 2020. 2
- [54] Kim Sung-Bin, Lee Hyun, Da Hye Hong, Suekyeong Nam, Janghoon Ju, and Tae-Hyun Oh. Laughtalk: Expressive 3d talking head generation with laughter. In *IEEE/CVF Winter Conference on Applications of Computer Vision, WACV 2024, Waikoloa, HI, USA, January 3-8, 2024*, pages 6392–6401. IEEE, 2024. 3
- [55] Shuai Tan, Bin Ji, Mengxiao Bi, and Ye Pan. Edtalk: Efficient disentanglement for emotional talking head synthesis. In *European Conference on Computer Vision*, pages 398–416. Springer, 2025. 2, 5, 6
- [56] Linrui Tian, Qi Wang, Bang Zhang, and Liefeng Bo. Emo: Emote portrait alive – generating expressive portrait videos with audio2video diffusion model under weak conditions, 2024. 1
- [57] Thomas Unterthiner, Sjoerd van Steenkiste, Karol Kurach, Raphael Marinier, Marcin Michalski, and Sylvain Gelly. Towards accurate generative models of video: A new metric and challenges, 2019. 5
- [58] Konstantinos Vougioukas, Stavros Petridis, and Maja Pantic. Realistic speech-driven facial animation with gans. *International Journal of Computer Vision*, pages 1–16, 2019. 1, 2
- [59] Cong Wang, Kuan Tian, Jun Zhang, Yonghang Guan, Feng Luo, Fei Shen, Zhiwei Jiang, Qing Gu, Xiao Han, and Wei Yang. V-express: Conditional dropout for progressive training of portrait video generation. *CoRR*, abs/2406.02511, 2024. 2, 6, 1
- [60] Kaisiyuan Wang, Qianyi Wu, Linsen Song, Zuoqian Yang, Wayne Wu, Chen Qian, Ran He, Yu Qiao, and Chen Change Loy. Mead: A large-scale audio-visual dataset for emotional talking-face generation. In *ECCV*, 2020. 5, 6
- [61] Ting-Chun Wang, Arun Mallya, and Ming-Yu Liu. One-shot free-view neural talking-head synthesis for video conferencing. In *Proceedings of the IEEE/CVF conference on computer vision and pattern recognition*, pages 10039–10049, 2021. 1
- [62] Zheyu Wang, Jieying Zheng, and Feng Liu. Improvement of continuous emotion recognition of temporal convolutional networks with incomplete labels. *IET Image Processing*, 18(4):914–925, 2024. 2
- [63] Huawei Wei, Zejun Yang, and Zhisheng Wang. Aniportrait: Audio-driven synthesis of photorealistic portrait animation, 2024. 1, 2, 6
- [64] Chao Xu, Shaoting Zhu, Junwei Zhu, Tianxin Huang, Jiangning Zhang, Ying Tai, and Yong Liu. Multimodal-driven talking face generation via a unified diffusion-based generator. *CoRR*, abs/2305.02594, 2023. 2
- [65] Mingwang Xu, Hui Li, Qingkun Su, Hanlin Shang, Liwei Zhang, Ce Liu, Jingdong Wang, Yao Yao, and Siyu Zhu. Hallo: Hierarchical audio-driven visual synthesis for portrait image animation, 2024. 1, 2, 6
- [66] Sicheng Xu, Guojun Chen, Yu-Xiao Guo, Jiaolong Yang, Chong Li, Zhenyu Zang, Yizhong Zhang, Xin Tong, and Baining Guo. Vasa-1: Lifelike audio-driven talking faces generated in real time. *arXiv preprint arXiv:2404.10667*, 2024. 2
- [67] Zhihao Xu, Shengjie Gong, Jiapeng Tang, Lingyu Liang, Yining Huang, Haojie Li, and Shuangping Huang. Kmtalk: Speech-driven 3d facial animation with key motion embedding. In *Computer Vision - ECCV 2024 - 18th European Conference, Milan, Italy, September 29-October 4, 2024, Proceedings, Part LVI*, pages 236–253. Springer, 2024. 2
- [68] Dogukan Yaman, Fevziye Irem Eyiokur, Leonard Bärmann, Seymanur Akti, Hazim Kemal Ekenel, and Alexander Waibel. Audio-visual speech representation expert for enhanced talking face video generation and evaluation. In *IEEE/CVF Conference on Computer Vision and Pattern Recognition, CVPR 2024 - Workshops, Seattle, WA, USA, June 17-18, 2024*, pages 6003–6013. IEEE, 2024. 5
- [69] Shengming Yin, Chenfei Wu, Huan Yang, Jianfeng Wang, Xiaodong Wang, Minheng Ni, Zhengyuan Yang, Linjie Li, Shuguang Liu, Fan Yang, Jianlong Fu, Ming Gong, Lijuan Wang, Zicheng Liu, Houqiang Li, and Nan Duan. NUWA-XL: diffusion over diffusion for extremely long video generation. In *Proceedings of the 61st Annual Meeting of the Association for Computational Linguistics (Volume 1: Long Papers), ACL 2023, Toronto, Canada, July 9-14, 2023*, pages 1309–1320. Association for Computational Linguistics, 2023. 2
- [70] Jianhui Yu, Hao Zhu, Liming Jiang, Chen Change Loy, Weidong Cai, and Wayne Wu. CelebV-Text: A large-scale facial text-video dataset. In *CVPR*, 2023. 5, 6, 2
- [71] Chenxu Zhang, Chao Wang, Jianfeng Zhang, Hongyi Xu, Guoxian Song, You Xie, Linjie Luo, Yapeng Tian, Xiaohu Guo, and Jashi Feng. Dream-talk: diffusion-based realistic emotional audio-driven method for single image talking face generation. *arXiv preprint arXiv:2312.13578*, 2023. 2

- [72] David Junhao Zhang, Jay Zhangjie Wu, Jia-Wei Liu, Rui Zhao, Lingmin Ran, Yuchao Gu, Difei Gao, and Mike Zheng Shou. Show-1: Marrying pixel and latent diffusion models for text-to-video generation, 2023. 4
- [73] Lvmin Zhang, Anyi Rao, and Maneesh Agrawala. Adding conditional control to text-to-image diffusion models. In *Proceedings of the IEEE/CVF International Conference on Computer Vision*, pages 3836–3847, 2023. 2
- [74] Richard Zhang, Phillip Isola, Alexei A. Efros, Eli Shechtman, and Oliver Wang. The unreasonable effectiveness of deep features as a perceptual metric. In *2018 IEEE Conference on Computer Vision and Pattern Recognition, CVPR 2018, Salt Lake City, UT, USA, June 18-22, 2018*, pages 586–595. Computer Vision Foundation / IEEE Computer Society, 2018. 5
- [75] Wenxuan Zhang, Xiaodong Cun, Xuan Wang, Yong Zhang, Xi Shen, Yu Guo, Ying Shan, and Fei Wang. Sadtalker: Learning realistic 3d motion coefficients for stylized audio-driven single image talking face animation. In *IEEE/CVF Conference on Computer Vision and Pattern Recognition, CVPR 2023, Vancouver, BC, Canada, June 17-24, 2023*, pages 8652–8661. IEEE, 2023. 2, 6
- [76] Zhimeng Zhang, Lincheng Li, Yu Ding, and Changjie Fan. Flow-guided one-shot talking face generation with a high-resolution audio-visual dataset. In *2021 IEEE/CVF Conference on Computer Vision and Pattern Recognition (CVPR)*, pages 3660–3669, 2021. 5, 6, 7, 8, 2
- [77] Hang Zhou, Yasheng Sun, Wayne Wu, Chen Change Loy, Xiaogang Wang, and Ziwei Liu. Pose-controllable talking face generation by implicitly modularized audio-visual representation. In *Proceedings of the IEEE/CVF conference on computer vision and pattern recognition*, pages 4176–4186, 2021. 2
- [78] Hao Zhu, Wayne Wu, Wentao Zhu, Liming Jiang, Siwei Tang, Li Zhang, Ziwei Liu, and Chen Change Loy. CelebV-HQ: A large-scale video facial attributes dataset. In *ECCV*, 2022. 5, 2

KeyFace: Expressive Audio-Driven Facial Animation for Long Sequences via KeyFrame Interpolation

Supplementary Material

A. Model Details

Implementation In our experiments, both the keyframe generator and the interpolation model produce sequences of 14 frames. The keyframes are spaced by $S = 12$ frames, and the interpolation model uses two frames as conditioning. Consequently, the total number of new frames generated through interpolation is S . This configuration captures extended temporal dependencies while maintaining computational efficiency.

We initialize the weights of the U-Net and VAE from SVD [3] and conduct all experiments on NVIDIA A100 GPUs with a batch size of 32 for both models. The keyframe generator is trained for 60,000 steps, while the interpolation model requires 120,000 steps due to its greater deviation from the pre-trained SVD. We use the AdamW optimizer [40] with a constant learning rate of 1×10^{-5} , following a 1,000-step linear warm-up. For inference, we use 10 steps, consistent with [4]. During training, the identity frame is randomly selected from each video clip.

Audio is sampled at 16,000 Hz to align with the pre-trained encoders (WavLM [8] and BEATs [9]), while video frames are extracted at 25 fps and resized to 512×512 pixels. During training, the audio condition is randomly dropped 20 % of the time, and the identity condition is dropped 10 % of the time to strengthen the guidance effect.

We train the reduced model for autoguidance [32] with 16× fewer training steps. The default settings are summarized in Table 8.

Parameter	Value
Keyframe sequence length (T)	14
Keyframe spacing (S)	12
Interpolation sequence length (S)	12
Keyframe training steps	60,000
Interpolation training steps	120,000
Training batch size	32
Optimizer	AdamW
Learning rate	1×10^{-5}
Warm-up steps	1,000
Inference steps	10
GPU used	NVIDIA A100
Autoguidance [32] model training steps	$120,000 / 16 = 7,500$
Audio condition drop rate for CFG [21]	20 %
Identity condition drop rate for CFG [21]	10 %

Table 8. Default model parameters and training configurations.

Inference speed One limitation of our model is that it does not yet support real-time generation. Nevertheless, our two-stage approach is faster than competing diffusion-based models, particularly because it allows batching, unlike autoregressive methods. We present an inference speed comparison (Table 9), measured in seconds per frame. Real-time inference could potentially be achieved through distillation methods (e.g., UFOGen), which we leave for future work.

V-Express [59]	Hallo [65]	AniPortrait [63]	EchoMimic [11]	Keyface
3.36	1.9	0.44	0.76	0.26

Table 9. Seconds per frame comparison for baseline models.

B. Comparison with SVD

Our method builds upon Stable Video Diffusion (SVD) [3] by introducing carefully designed architectural and task-specific adaptations. These modifications distinctly set our approach apart from prior work. We highlight the primary differences below.

Audio Conditioning While SVD primarily conditions on the initial frame to predict subsequent video frames, our method extends this capability by conditioning on both an identity frame and audio inputs to drive video generation. To the best of our knowledge, we are the first to employ conditioning based on outputs from two distinct audio encoders (WavLM [8] and BEATs [9]), allowing simultaneous processing of speech and non-speech audio.

Emotional Conditioning Unlike the original SVD architecture, our approach incorporates additional control over emotional expression. We demonstrate that training emotional models exclusively with pseudo-labels for valence and arousal achieves robust and consistent performance.

Loss Functions SVD employs only the EDM loss [31]. In contrast, we use two additional pixel-space losses along with a weighted loss that specifically targets the lower region of generated images.

Guidance Whereas SVD solely employs vanilla classifier-free guidance (CFG) [21], we provide an in-depth investigation into optimal guidance techniques

tailored specifically to each stage of our pipeline. We found that, for the keyframe model, assigning different CFG weights to identity and audio conditions leads to better performance and improved robustness compared to classical CFG. Additionally, since interpolation requires greater flexibility in head movement, we employed autoguidance [32] to dynamically balance guidance, resulting in enhanced overall video quality.

C. Datasets

C.1. Data details

Table 10 provides an overview of the datasets used in this paper, detailing the number of speakers, videos, average video duration, and total duration for each dataset. We use a combination of publicly available datasets (HDTF [76], CelebV-HQ [78], CelebV-Text [70]) and our own collected data. As stated in the main paper, we use only HDTF and the collected data for training our final model. Additionally, we utilize reference frames from FEED [14] for some qualitative results.

Dataset	# Speakers	# Videos	Duration	
			Avg. (sec.)	Total (hrs.)
HDTF [76]	264	318	139.08	12
CelebV-HQ [78]	3,668	12,000	4.00	13
CelebV-Text [70]	9,109	75,307	6.38	130
Collected data	824	4,677	123.15	160
Collected data (NSV)	639	5,701	18.94	30

Table 10. Overview of the datasets used in the study.

C.2. Preprocessing details

Even during our experimentation with alternative data sources in the data ablation study, we aim to obtain the highest-quality data possible. To achieve this, we propose a data preprocessing pipeline with the following steps:

- Extract 25 fps video and 16 kHz mono audio.
- Discard low-quality videos based on a quality score computed using HyperIQA [53].
- Detect and separate scenes using PySceneDetect.
- Remove clips without active speakers using Light-ASD [39].
- Estimate landmarks and poses using face-alignment.
- Crop the video around the facial region across all frames.

Using this pipeline, we curate CelebV-HQ [78] and CelebV-Text [70].

However, even after filtering the datasets, we found that many samples contain editing effects and/or occlusions that are not detected. Examples include visible hands, camera movement, editing effects, and occlusions, which we found occur in 20 % of videos even after our cleaning process, as illustrated in Figure 9. Since these artefacts don't correlate

with speech, they can't be replicated by the model, hindering performance as shown in Section 5.3.



Figure 9. Illustration of bad examples in CelebV-HQ [78] and CelebV-Text [70].

D. Evaluation metrics

D.1. LipScore

To evaluate the effectiveness of our proposed LipScore metric compared to the traditional SyncNet metric, we conduct experiments introducing controlled temporal and spatial perturbations to synchronized audio-visual data. The goal is to observe how each metric responds to these perturbations and determine which better correlates with the expected degradation in lip synchronization quality.

Temporal misalignment sensitivity In the first set of experiments, we introduce temporal misalignments by shifting the ground truth video temporally. The time shifts range from 0 milliseconds (ms) to 1000 ms.

Figure 10 illustrates the behavior of SyncNet Confidence and SyncNet Distance as functions of the time shift. We observe that SyncNet Confidence and Distance remain constant up to approximately 400 ms and only start to change significantly beyond this point. This behavior is undesirable, as even small misalignments (e.g., 100–200 ms) should result in a noticeable decrease in confidence and an increase in distance.

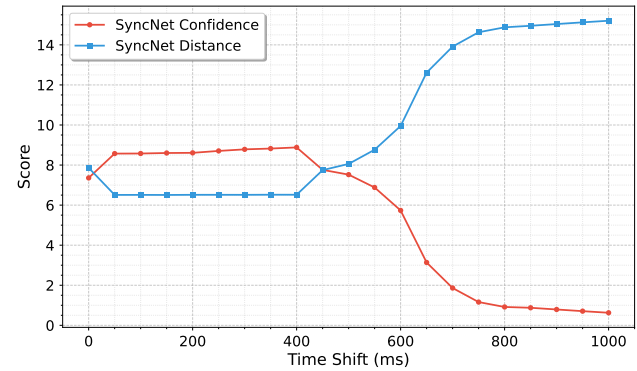


Figure 10. SyncNet Confidence and SyncNet Distance as functions of time shift (ms).

In contrast, Figure 11 shows the LipScore metric's response to the same range of time shifts. LipScore exhibits a

stable and consistent decrease in score as the time shift increases. It begins to penalize even small temporal perturbations, with a sharp decline at smaller offsets, and stabilizes at lower scores as larger misalignments are introduced. This behavior aligns with the expected characteristics of a robust lip synchronization metric, demonstrating continuous sensitivity to temporal misalignments without erratic or overly abrupt changes.

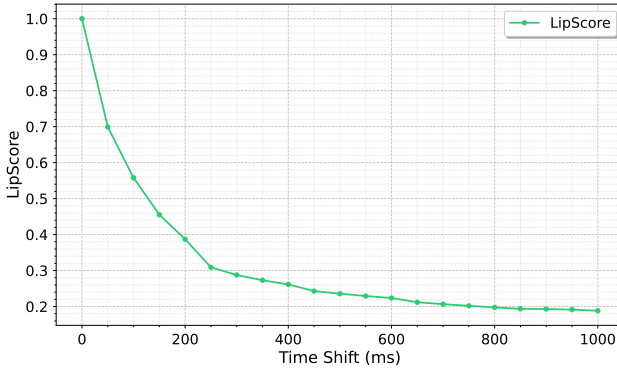


Figure 11. LipScore as a function of time shift (ms).

Robustness to spatial perturbations We evaluate the robustness of the metrics to spatial transformations by introducing horizontal shifts and rotations to the video frames.

Figure 12 illustrates the percentage deviation from the initial metric values as horizontal shifts increase. LipScore remains stable, exhibiting minimal deviation across the range of horizontal shifts, indicating its robustness to this type of spatial perturbation. In contrast, SyncNet Confidence and SyncNet Distance show significant deviations starting at a shift of 75 pixels, highlighting their sensitivity to horizontal displacements.

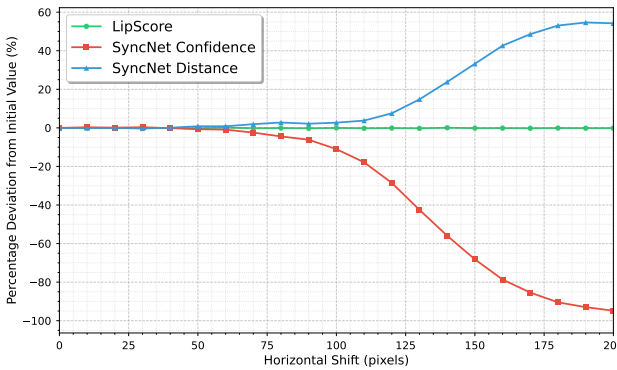


Figure 12. Effect of horizontal shifts on LipScore, SyncNet Confidence, and SyncNet Distance. The plot shows the percentage deviation from the initial value as the horizontal shift increases.

Similarly, Figure 13 shows the percentage deviation in

metric values as the rotation angle of the video frames increases. LipScore again demonstrates robustness, with negligible changes in its values even as the rotation angle grows. In contrast, SyncNet Confidence and SyncNet Distance exhibit substantial deviations starting at 20 degrees, indicating that these metrics are more adversely affected by rotational transformations.

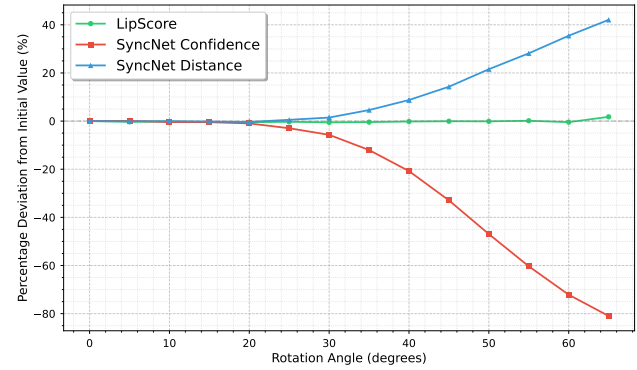


Figure 13. Effect of rotation angles on LipScore, SyncNet Confidence, and SyncNet Distance. The plot shows the percentage deviation from the initial value as the rotation angle increases.

WER on unseen datasets We additionally evaluate our state-of-the-art lipreader [41] on HDTF and find that it achieves a 21 % WER, demonstrating strong performance on unseen data and further supporting LipScore’s validity.

D.2. Non-speech vocalization classifier

We introduce the Non-Speech Vocalization (NSV) Classifier as part of our evaluation methodology. This not only highlights the limitations of pre-trained speech-driven animation methods but also demonstrates the capabilities of our model in generating realistic NSV sequences. The model processes video inputs and classifies them into one of eight NSV types, plus speech.

Architecture The architecture of the system is presented in Fig. 14. We employ a Multiscale Vision Transformer (MViTv2) [37] backbone, augmented with two linear layers and a dropout layer with a dropout probability set to 0.2. The MViTv2 model, pre-trained on the Kinetics dataset [33], achieves a top-5 accuracy of 94.7 %.

Training Our model is trained using a dataset containing video clips of eight different NSV types and speech. The eight NSV classes are: “Mhm”, “Oh”, “Ah”, coughs, sighs, yawns, throat clears, and laughter. During the training process, video clips corresponding to any of these classes are fed into the model. We train using the AdamW

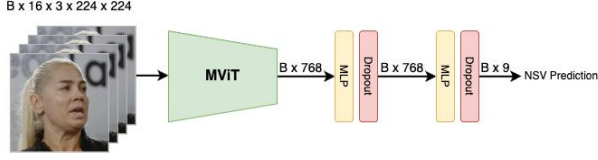


Figure 14. The architecture used for the Non-Speech Vocalization Classifier. The batch size is denoted as B .

optimizer with a learning rate of 1×10^{-4} , $\beta_1 = 0.9$, and $\beta_2 = 0.999$. The cross-entropy loss is employed as the loss function.

Our model achieves an F1 score of 0.7 across these nine classes, demonstrating its effectiveness in classifying various NSVs and speech.

NSVs performance boundaries To demonstrate and understand the effectiveness of NSV_{acc} across individual NSVs, we present a confusion matrix on the validation set of the data used to train NSV_{acc} (Fig. 15, left). Although the model achieves good overall performance, certain NSVs are frequently confused, such as “Oh” with “Ah,” “Sigh” with “Mhm,” and “Yawn” with “Cough.”

Additionally, we demonstrate that our model can generate visually distinct NSVs (Fig. 15, right) with few confusions by generating 10 videos per NSV category and speech.

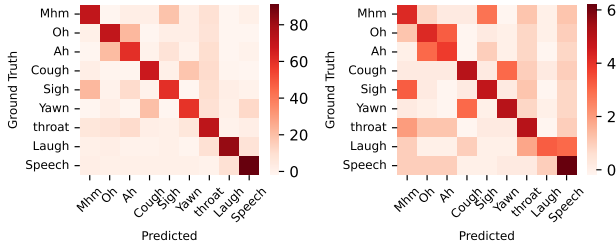


Figure 15. NSV confusion matrix for generated (left) and validation (right) videos.

E. User study details

To evaluate the performance of our proposed method, KeyFace, against existing baselines, we conduct a comprehen-

sive user study. Participants view pairs of talking face videos and select the one they find more realistic. This section summarizes the results of the pairwise comparisons and the derived metrics.

Pairwise Win Rates: The pairwise win rate matrix is presented in Figure 16. Each cell represents the proportion of times the reference model (rows) is preferred over the competing model (columns). Green indicates a high win rate for the reference model, while red represents a lower win rate. KeyFace is consistently preferred over baseline models, achieving a win rate of at least 64 % against all other models.

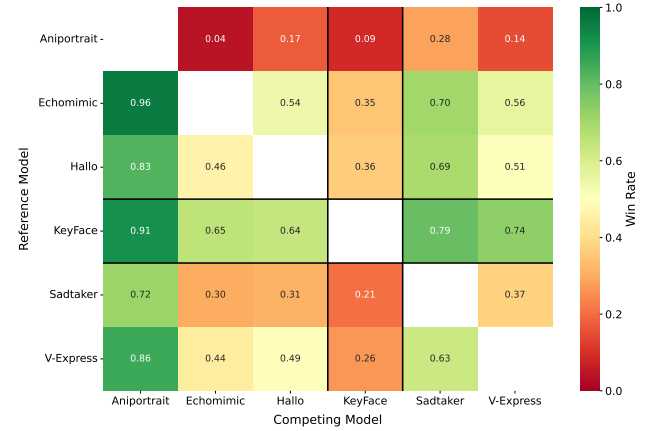


Figure 16. Pairwise win rates between reference (rows) and competing models (columns). Green indicates higher, Red lower win rates.

Elo ratings: Figure 17 presents the Elo ratings for all models with 95 % confidence intervals. KeyFace achieves the highest Elo rating, significantly outperforming the baselines, demonstrating its effectiveness in generating high-quality talking face animations.

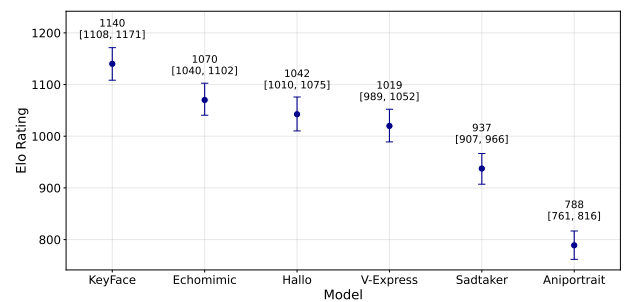


Figure 17. Elo ratings for all models with 95 % confidence intervals. Higher ratings indicate better overall performance.

Elo rating distributions: The density distributions of Elo ratings are shown in Figure 18. KeyFace exhibits a sharp, high-density peak at the upper end, highlighting its robustness and consistent user preference across evaluation scenarios. Echomimic, V-Express, and Hallo show significant overlap in their results, while Aniportrait and SadTalker consistently receive lower ratings.

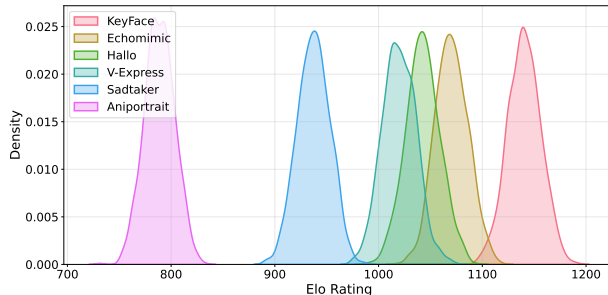


Figure 18. **Density distributions of Elo ratings for all models.** Peaks indicate the most probable performance levels, with higher ratings reflecting better performance.

F. Additional ablation

Method	FID ↓	FVD ↓	LipScore ↑
w/o cross attention	16.95	167.39	0.35
w/o timestep	17.20	176.83	0.28
cross attention + timestep	16.76	137.25	0.36

Table 11. **Audio conditioning ablation** on HDTF [76]: “Cross attention” refers to incorporating audio through a cross-attention mechanism, while “timestep” refers to adding the audio embeddings to the timestep embeddings. The best results are highlighted in **bold** and default settings are highlighted in gray on all tables.

Audio mechanisms Table 11 presents an ablation study on the impact of different audio conditioning mechanisms on video generation quality. The results show that the audio timestep plays a critical role in achieving accurate lip synchronization, as removing it (row “w/o timestep”) results in the lowest LipScore and the highest FVD. Adding cross attention alone improves video quality but only marginally enhances the LipScore compared to when the timestep is absent. The best performance is achieved when both cross attention and audio timestep embeddings are used together, leading to the lowest FID, significantly lower FVD, and the highest LipScore. This indicates that while audio timestep embeddings are essential for achieving good lip synchronization, the addition of cross attention further enhances the overall quality of the generated videos by improving visual coherence and temporal consistency.

Training on HDTF only To ensure a fair comparison with baseline models, we retrain our model exclusively on publicly available data (i.e. HDTF [76]), removing all non-public sources. Although this leads to a decrease in performance, our model still outperforms baseline methods trained on larger datasets. We emphasize that most existing methods rely on private datasets; therefore, to maintain fairness, we curated our dataset to have comparable scale in terms of total hours and number of speakers as described in Section C.1.

Method	FID ↓	FVD ↓	LipScore ↑
KeyFace (HDTF only)	19.49	165.06	0.28

Table 12. Results of pipeline trained on HDTF only.

G. Limitations

One key limitation of our model, which it shares with all baseline methods, is its performance when the initial frame exhibits an extreme head pose. This issue primarily stems from the lack of training data containing such extreme poses, resulting in difficulties in reconstructing the occluded or unseen parts of the face. As illustrated in Figure 19, although the model can generate plausible videos with accurate lip synchronization, it partially loses the identity of the reference image in these scenarios. Additional failure cases involving challenging reference frames are provided in the supplementary videos.



Figure 19. An example showcasing KeyFace’s limitations in handling extreme head poses.

H. Additional qualitative results

To further demonstrate the effectiveness of our method, we provide **example videos generated by KeyFace** (as well as competing methods, for comparison) in the supplementary material:

- **Non-speech vocalizations comparison.** We evaluate the model’s ability to handle eight distinct NSVs and compare its performance with baseline methods, highlighting the limitations of current state-of-the-art models and the strengths of our approach. For a fair comparison, all examples maintain a neutral emotional tone.
- **Speech and NSV comparison.** We demonstrate the model’s capability to generate both speech and NSVs

within the same video, comparing its performance to other approaches. The results showcase the holistic nature of our method, particularly in contrast to baseline models. We maintain a neutral emotional tone for consistency.

- **Side-by-side comparison.** We present side-by-side comparisons between KeyFace and baseline models, showcasing KeyFace’s superior performance in generating realistic and expressive facial animations.
- **Emotion interpolation.** We showcase transitions between different emotional states, emphasizing the model’s ability to capture subtle and nuanced expressions.
- **Out-of-distribution robustness.** Figure 20 illustrates the model’s robustness in handling non-human faces, demonstrating successful generalization to a variety of input conditions.
- **Expanded KeyFace examples.** We provide additional videos featuring KeyFace-generated animations in English and other languages, highlighting the model’s generalization capabilities across different linguistic contexts.



Figure 20. We present a set of examples with **out-of-distribution** reference frames.